Probing spontaneously symmetry-broken phases with spin-charge separation through noise correlation measurements

Letter

Probing spontaneously symmetry-broken phases with spin-charge separation through noise correlation measurements

Kerman Gallego-Lizarribar,[1] Sergi Julià-Farré,[2] Maciej Lewenstein,[2,3] Christof Weitenberg,[4,5,6] Luca Barbiero,[7] and Javier Argüello-Luengo[1,2,*]

[1]*Departament de Física, Universitat Politécnica de Catalunya, Campus Nord B4-B5, 08034 Barcelona, Spain*

[2]*ICFO - Institut de Ciencies Fotoniques, Barcelona Institute of Science and Technology, Avenida Carl Friedrich Gauss 3, 08860 Castelldefels (Barcelona), Spain*

[3]*ICREA, Passeig Lluís Companys 23, 08010 Barcelona, Spain*

[4]*Department of Physics, TU Dortmund University, 44227 Dortmund, Germany*

[5]*Institut für Quantenphysik, Universität Hamburg, 22761 Hamburg, Germany*

[6]*Hamburg Centre for Ultrafast Imaging, 22761 Hamburg, Germany*

[7]*Institute for Condensed Matter Physics and Complex Systems, DISAT, Politecnico di Torino, I-10129 Torino, Italy*

(Received 23 April 2024; revised 11 July 2024; accepted 12 September 2024; published 22 November 2024)

Spontaneously symmetry-broken (SSB) phases are locally ordered states of matter characterizing a large variety of physical systems. Because of their specific ordering, their presence is usually witnessed by means of local order parameters. Here, we propose an alternative approach based on statistical correlations of noise after the ballistic expansion of an atomic cloud. We indeed demonstrate that probing such noise correlators allows one to discriminate among different SSB phases characterized by spin-charge separation. As a particular example, we test our prediction on a 1D extended Fermi-Hubbard model, where the competition between local and nonlocal couplings gives rise to three different SSB phases: a charge density wave, a bond-ordering wave, and an antiferromagnet. Our numerical analysis shows that this approach can accurately capture the presence of these different SSB phases, thus representing an alternative and powerful strategy to characterize strongly interacting quantum matter.

DOI: 10.1103/PhysRevResearch.6.L042048

Introduction. Symmetries play a central role in the characterization of the microscopic properties of the large majority of quantum systems [1–3]. In this regard, the Mermin-Wagner-Hohenberg theorem [4,5] demonstrates that, under specific conditions, interacting processes can lead to the formation of the, so called, spontaneously symmetry-broken (SSB) phases. Here, the mechanism of symmetry breaking manifests in the appearance of locally ordered states of matter that are captured by specific local order parameters (LOPs) [6]. While theoretical analysis made an extensive use of LOPs, the experimental characterization of SSB phases represented a more challenging task. Nevertheless, the advent of ultracold atomic quantum simulators [7,8] allowed for the investigation of SSB regimes to finally flourish, as proved by the detection of equilibrium [9] and out-of-equilibrium [10] density waves, supersolids [11–13], and antiferromagnets [14–16]. In this regard, two main aspects of ultracold experimental platforms proved particularly important: the impressive versatility in the engineering of Hamiltonians, and the highly accurate detection techniques that allow one to probe local ordering. Specific to this last point, quantum gas microscopy [17] represents an extremely complex and powerful method capable of probing both density [18,19] and spin [14,20] local distributions, where first fundamental results [21,22] have been obtained. Regarding the tailored interactions, the study of SSB states would benefit from sizable nonlocal interactions, whose engineering with dipolar atoms requires the use of lattices with ultrashort lattice spacing [9,23]. Although interesting proposals are present [24,25], the diffraction limit might drastically challenge the effectiveness of quantum gas microscopes to detect these phases, which leads to an open quest for less demanding detection schemes.

Techniques based on time-of-flight (TOF) measurements offer an alternative, as they allow the extraction of noise correlation measurements (NCMs) from spatial density-density correlations after a ballistic expansion of the gas [26], which does not require a single-site imaging of the lattice. Through such technique, different states of matter have already been efficiently detected [27–31]. In this Letter, we demonstrate that NCMs can as well be highly effective in revealing the presence of SSB phases that are characterized by spin-charge separation [32–34]. Specifically, we first derive the expressions that show that NCMs are able to capture the three possible SSB phases occurring in 1D spinful fermionic systems, which are always characterized by gapped charge and spin excitation spectra [35,36]. These are a charge density wave (CDW), an antiferromagnet (AFM), and a bond order wave (BOW) with broken site inversion symmetry, as

*Contact author: javier.arguello.luengo@upc.edu

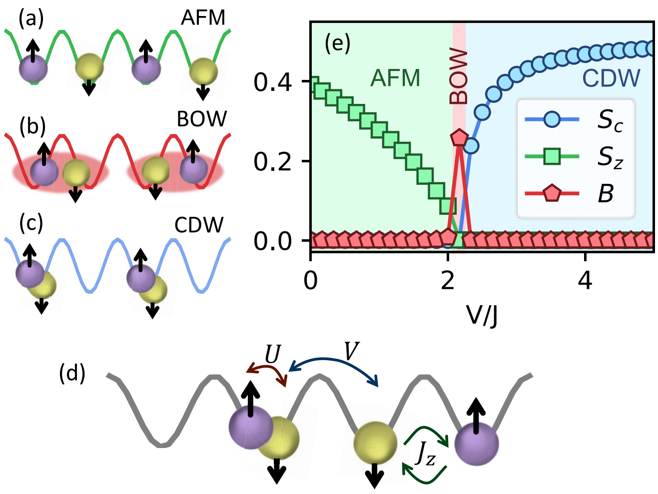

FIG. 1. Illustration of the AFM (a), BOW (b), and CDW (c) phases. (d) Schematic representation of the 1D EFH model (4) at half occupation. Atoms of different spin are illustrated with different colors and two-point arrows indicate on-site (U) and nearest-neighbor (V) interactions. An additional term (J_z) couples the spin of neighbor sites. (e) Phase diagram associated to the ground state of the EFH model in the thermodynamic limit. As the value of V/J increases, one observes the transition between the AFM, BOW, and CDW phases (colored in green, red, and blue, respectively). See Supplemental Material Ref. [37] for further details. Parameters: $U = 4J$ and $J_z = 0.5J$.

represented in Figs. 1(a)–1(c). Notably, while the local ordering of CDW and AFM appears at the level of lattice sites, in the BOW it takes place in bonds connecting consecutive sites, whose detection is the subject of ongoing efforts for quantum gas microscopy [38,39]. The alternative use of NCMs to detect this phase had not been proposed before. Based on such a fundamental aspect, we then test our predictions on an extended Fermi-Hubbard (EFH) model where the aforementioned regimes can be engineered. Here, our numerical analysis for system sizes similar to those of current experiments [9] demonstrates that NCMs provide a ground-state characterization that accurately agrees with the one derived through LOPs, while not relying on spatially resolving the optical lattice. Our results thus provide insights toward a more complete understanding and characterization of SSB phases of matter.

NCM for SSB phases. The NCM can be accessed by a sudden release of the optical trap and a posterior fluorescence measurement once the atoms, of mass m, have expanded beyond the characteristic size of the lattice during a finite time τ [26]. After this ballistic expansion, each momentum is associated to detection in position $x_\nu = \hbar p_\nu \tau/m$, where $p_\nu = p + 2\nu k$, ν is an integer number, and $k = 2\pi/\lambda$ depends on the wavelength of the lattice geometry. The Pauli principle then prevents the simultaneous detection $\langle \hat{n}_\sigma(x) \cdot \hat{n}_\sigma(x')\rangle$ at distances, $d = x' - x$, which are multiples of $\ell = (2\hbar k)\tau/m$. After normalizing by the case of independent detection $\langle \hat{n}(x)\rangle\langle \hat{n}(x')\rangle$, the NCM writes as

$$\mathcal{N}(d) = 1 - \frac{\int dx \langle \hat{n}(x + d/2) \cdot \hat{n}(x - d/2)\rangle}{\int dx \langle \hat{n}(x + d/2)\rangle\langle \hat{n}(x - d/2)\rangle}, \quad (1)$$

where the bracket notation, $\langle\cdot\rangle$, indicates the statistical averaging over the region where fluorescence is detected. In this work, whenever we omit explicitly the spin index we refer to the sum over both spins, $\hat{n} = \hat{n}_\uparrow + \hat{n}_\downarrow$.

Interestingly, the presence of peaks in the NCM can reveal symmetries of the state that are associated to structural order in the chain [40,41], thus unveiling the presence of SSB phases. One of these examples is the CDW, which is characterized by a broken translational symmetry that manifests as a perfect alternation between empty and doubly occupied sites. Notably, charge excitations become gapped due to density modulation, while the on-site pairing also generates gapped spin excitations. In a bipartite lattice picture, this manifests as a different site occupation, taking values $n_{e/o,\sigma}$ on each even/odd site for spin $\sigma \in \{\uparrow, \downarrow\}$, which results in a NCM of the form [37]

$$\mathcal{N}(\nu\ell/2) = \sum_\sigma [n_{e\sigma} + (-1)^\nu n_{o\sigma}]^2 \Big/ \Big[\sum_\sigma (n_{e\sigma} + n_{o\sigma})\Big]^2. \quad (2)$$

In analogy to measurements in 2D systems with imposed broken symmetry [31], $\mathcal{N}(\ell/2)$ is null for a homogeneous distribution, and nonvanishing for a bipartite occupation. Therefore, the NCM in Eq. (2) serves as a rigorous probe that is capable of detecting translational symmetry broken phases. In the case of a spinful fermionic CDW occurring in half-filled 1D lattices, we then expect $n_{e\sigma} = 1$ and $n_{o\sigma} = 0$, so that the NCM saturates to $\mathcal{N}(\ell/2) = 0.5$.

Interestingly, such analysis is also relevant for the characterization of the AFM SSB phase represented in Fig. 1(a). This phase exhibits a finite charge gap that originates from energetically prevented local pairing, while the perfect spatial alternation between $\uparrow$ and $\downarrow$ particles translates into gapped spin excitations. For the half-filled fermionic system described above, the AFM state, $n_{o\uparrow} = n_{e\downarrow} = 1$ and $n_{o\downarrow} = n_{e\uparrow} = 0$, saturates again the NCM in Eq. (2) to the value $\mathcal{N}(\ell/2) = 0.5$.

In these two SSB phases, local order is present at the level of lattice sites. In contrast to this, the BOW phase occurring in different fermionic chains [35,42,43] is characterized by the ordering of local bonds, $b_{r\sigma} = \langle \hat{c}^\dagger_{r\sigma}\hat{c}_{r+1\sigma} + \text{H.c.}\rangle$, which results in a spontaneously generated lattice dimerization [see Fig. 1(b)]. In analogy to AFM, the charge gap in the BOW reflects in a uniform distribution of singly occupied lattice sites, while the lattice dimerization gives rise to the formation of singlets in neighboring sites causing spin-gapped excitations. Interestingly, the local ordering in the bonds translates into additional terms in the NCM [37],

$$\mathcal{N}(\nu\ell/2) = \frac{\sum_\sigma \big[\sum_r (-1)^{\nu r} n_{r\sigma}\big]^2 + 0.5\sum_\sigma \big[\sum_r (-1)^{\nu r} b_{r\sigma}\big]^2}{\big(\sum_{\sigma r} n_{r\sigma}\big)^2 - 0.5\big(\sum_{\sigma r} b_{r\sigma}\big)^2}. \quad (3)$$

In particular, in the SSB BOW we expect a different occupation of even/odd bonds, $n_{e/o,\sigma} = 0.5$, $b_{e\sigma} = 1$, $b_{o\sigma} = 0$, and one obtains a nonvanishing $\mathcal{N}(\ell/2) = 0.5$. Therefore, a nonzero value of $\mathcal{N}(\ell/2)$ in a fermionic chain indicates the presence of any of three possible symmetry breakings depicted in Fig. 1. In the following, we apply these results to a minimal model where the three SSB phases appear, and illustrate a strategy to rigorously detect individually each SSB phase by using NCMs.

SSB phases in the 1D EFH model. We consider a 1D EFH model describing a chain of length L where N spinful fermions, labeled by $\sigma = \uparrow, \downarrow$, interact through local U and nearest-neighbor V interactions [23], and are subject to an antiferromagnetic coupling $J_z > 0$ [see Fig. 1(d)] [44]:

$$\hat{H} = -J \sum_{\langle ij\rangle,\sigma} (\hat{c}^\dagger_{i\sigma}\hat{c}_{j\sigma} + \text{H.c.}) + V \sum_{\langle ij\rangle} \hat{n}_i \hat{n}_j + U \sum_{i=0}^{L-1} \hat{n}_{i\uparrow}\hat{n}_{i\downarrow} + J_z \sum_{\langle ij\rangle} \hat{S}^z_i \hat{S}^z_j, \quad (4)$$

where J parametrizes the nearest-neighbor hopping, and $\hat{S}^z_i = (\hat{n}_{i\uparrow} - \hat{n}_{i\downarrow})/2$. Here, we fix both the system density $N/L = 1$ and the total magnetization $\sum_i \hat{S}^z_i = 0$. For weak V, the on-site interaction dominates and the finite value of J_z turns out to be responsible for the breaking of the $SU(2)$ spin rotational symmetry, giving rise to the appearance of an AFM phase [45]. A strong nonlocal repulsion V causes that fermions in neighboring sites to become energetically unfavorable, which results in the formation of a CDW with broken translational symmetry [35,46]. For low enough J_z, the effective frustration generated in the regime $U \approx 2V$ turns out to be responsible for an effective Peierls instability that results in the formation of a SSB BOW [35].

The presence of the aforementioned SSB phases can be characterized by their respective LOP,

$$S_c = \frac{1}{L}\sum_i (-1)^i \langle \hat{n}_{i\uparrow} + \hat{n}_{i\downarrow}\rangle/2, \quad (5)$$

$$S_z = \frac{2}{L}\sum_i (-1)^i \langle \hat{S}^z_i\rangle, \quad (6)$$

$$B = \frac{2}{L}\sum_{i\sigma} (-1)^i b_{i\sigma}, \quad (7)$$

capturing the CDW, AFM, and BOW phases, respectively. For fixed values $U = 4J$ and $J_z = 0.5J$, our calculations of the LOPs in Fig. 1(e) confirm that the variation of V results in the appearance of the discussed SSB phases in the ground state of the EFH model (4) [47].

Discriminating among the different SSB phases through NCMs. So far, we have discussed that NCMs based on TOF measurements can probe the three SSB phases that appear in Eq. (4), but cannot directly discriminate among them in the reciprocal space where they operate. To circumvent this situation, we introduce a strategy where NCMs, in combination with tunable superlattices, can be used to reveal the presence of each SSB. For the ground state $|\psi_0\rangle$ of $\hat{H}$ and a symmetry of interest, we induce a time-dependent superlattice to reduce the energy of either of the possible charge or spin sectors associated to the symmetries of study. We will use the notations Ⓒ, Ⓐ, and Ⓑ for the superlattice modulation compatible with the order that spontaneously appears in the CDW, AFM, and BOW phase, respectively:

$$\hat{H}_{\text{Ⓒ}\,{}^{\text{e}}_{\text{o}}}(t) = -\Delta_{\text{T}}(t) \sum_{\sigma, i\in {}^{\text{even}}_{\text{odd}}} \hat{n}_{i\sigma}, \quad (8)$$

$$\hat{H}_{\text{Ⓐ}\,{}^{\text{e}}_{\text{o}}}(t) = -\Delta_{\text{T}}(t) \sum_{i\in {}^{\text{even}}_{\text{odd}}} (\hat{n}_{i\uparrow} - n_{i\downarrow}), \quad (9)$$

$$\hat{H}_{\text{Ⓑ}\,{}^{\text{e}}_{\text{o}}}(t) = \Delta_{\text{T}}(t) \sum_{\sigma} \sum_{i\in {}^{\text{even}}_{\text{odd}}} [\hat{c}^\dagger_{2i,\sigma}\hat{c}_{2i+1,\sigma} + \text{H.c.}]. \quad (10)$$

Here, we have defined $\Delta_{\text{T}}(t) = (t/T)^2\Delta$, where T is the total time of the passage, and the index e/o indicates whether the modulated Hamiltonian favors the occupation of even/odd sites [or bonds in the case of Ⓑ].

Let us now illustrate in greater detail how this strategy can assist distinguishing the discussed SSB phases. Starting with the CDW phase, in Figs. 2(b) and 2(c) we show the evolution of S_c and the noise correlator (respectively), as one starts from the ground state of the EFH model for a fixed value of $V = 5J$, where the CDW phase is present. The initial values $\mathcal{N}(\ell/2) \approx 0.5$ and $S_c \approx 0.5$ indicate the presence of the SSB phase where even sites are initially occupied. As we now shape the lattice to decrease the energy cost of occupying even sites, we observe at final time $TJ = 50$ no change in those values along the adiabatic evolution through the ground-state manifold of $\hat{H} + \hat{H}_{\text{Ⓒ},\text{e}}$ (continuous lines), which indicates that the SSB is unaltered. However, along the evolution with $\hat{H} + \hat{H}_{\text{Ⓒ},\text{o}}$ (dashed line) where the occupation of odd sites is favored, we observe that the state fails to reach adiabatically the state with opposite parity due to the closing of the gap along that path. As a consequence, the final values of the LOP and NCM do not saturate to 0.5, indicating that a state with broken symmetries has not been reached in this occasion. When looking into the final values of S_c after these two different paths in Fig. 2(a), we observe that this behavior holds for $V \gtrsim 2.25J$ (colored in blue, where the CDW phase is present) while, for $V \lesssim 2.25J$, the evolution along the even (continuous lines) and odd (dashed) adiabatic paths result into the same absolute values of S_c. Remarkably, this different evolution along the even and odd paths (8)–(10) schematized in Fig. 3(a) can also be sensed purely from NCMs. In the blue line of Fig. 3(b), we calculate the maximum difference $\Delta\mathcal{N}$ between the values of $\mathcal{N}(\ell/2)$ reached over time by those paths, which is null for $V \lesssim 2.25J$, while it is nonvanishing in the region $V \gtrsim 2.25J$, thus revealing the presence of the CDW phase without any need of LOPs or single-site resolution.

The applicability of this method is not restricted to CDWs, but it can also be used to detect AFM and BOW phases, as we illustrate in Figs. 2(d)–2(f) and Figs. 2(g)–2(i), by repeating the same analysis for the adiabatic passages $\hat{H}_{\text{Ⓐ}}(t)$, and $\hat{H}_{\text{Ⓑ}}(t)$, respectively. In the first case, we observe that the unequal evolution of S_z and the NCM [panels (e) and (f)] under the two parities of the path in Eq. (9) reveal the presence of an AFM phase for $V/J \lesssim 2.1$. Starting from the ground state of the EFH model for the latter case and $V/J = 2.16$, the BOW phase manifests from the different values of the bond-order LOP, and NCMs [panels (h) and (i)] reached by the system after the adiabatic suppression of tunneling in even or odd bonds (indicated with red continuous and dashed lines, respectively), following Eq. (10).

The presence of a specific SSB phase in the Hamiltonian thus manifests as a maximum discrepancy $\Delta\mathcal{N} \neq 0$, between the value of the NCM reached over time by the two possible

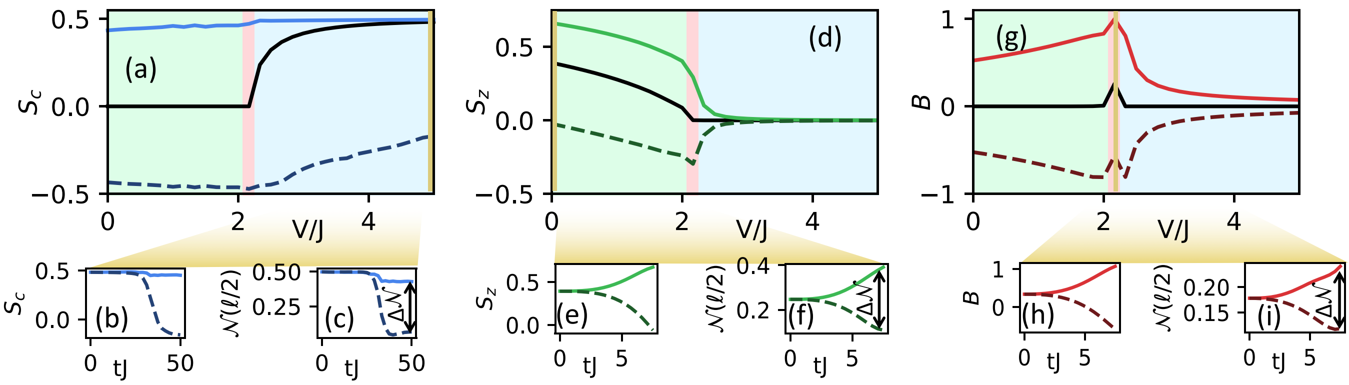

FIG. 2. (a) Black line follows the LOP associated to charge order (S_c) for different values of nearest-neighbor interaction strength, V/J. Blue lines indicate the final value of S_c after one adiabatically introduces the on-site dimerized energy shift in Eq. (8). Blue continuous line corresponds to the symmetry sector that is compatible with the initial sector of the ground state, and the dashed line corresponds to the opposite sector. Panels (b) and (c) indicate the evolution of S_c and $\mathcal{N}(\ell/2)$ (respectively) for a fixed $V/J = 5$ (yellow line). In (d) we focus on the LOP associated to antiferromagnetic order (S_z), represented in black. Continuous and dashed green lines show the final value of S_z for the even and odd adiabatic paths in Eq. (9). Panels (e) and (f) indicate S_z and $\mathcal{N}(\ell/2)$ (respectively) for $V/J = 0$ (yellow line). In (g) we follow the same approach for the LOP associated to bond order (B), represented in black. Continuous and dashed red lines show the final value of B after an adiabatic frustration of the tunneling in the bonds corresponding to the transformation (10) compatible with the ground state, or the opposite one, respectively. Panels (h) and (i) indicate the evolution of B and $\mathcal{N}(\ell/2)$ (respectively) for $V/J = 2.16$ (yellow line). Parameters: $U = 4J$, $J_z = 0.5J$, $\Delta = 10J$, 100 sites, and $TJ = 50$.

paths (e and o) associated to that symmetry [(8)–(10)]. One should note that, in an experiment, the SSB will be decided by an uncontrolled pinning potential and will be different in each realization. Therefore, the symmetry breaking will manifest as a bimodal distribution of measurement outcomes, where the separation $\Delta\mathcal{N}$ between the two peaks is the relevant measure. Remarkably, this magnitude, represented in Fig. 3(b), allows one to reconstruct the same phase diagram as the one obtained from LOP [see Fig. 1(e)].

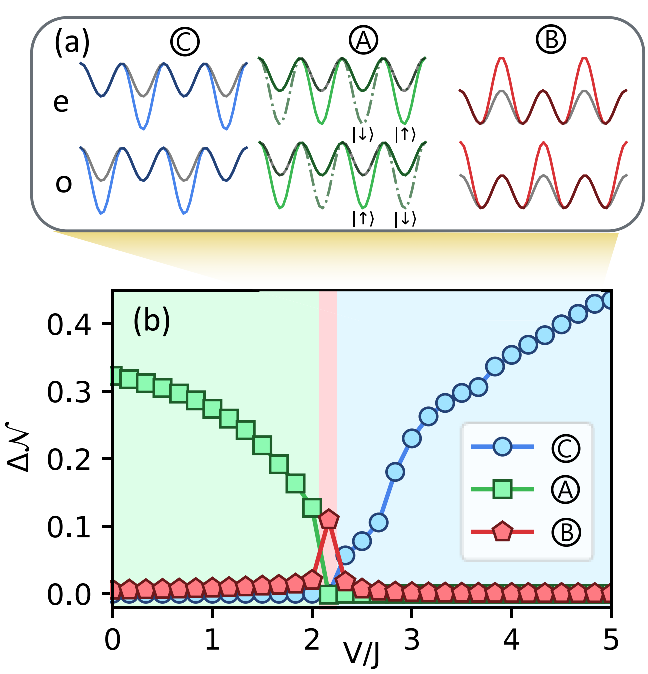

FIG. 3. (a) Schematic representation of the superlattices induced by the adiabatic transformations (8)–(10). (b) Difference in the NCM reached after the even or odd sector of those transformations reveals the presence of the CDW, AFM, and BOW phases of the EFH model (4) (see main text). Parameters as in Fig. 2.

Discussion and outlook. We have shown that noise correlation measurements can represent a fundamental tool in order to probe spontaneously symmetry broken phases with spin-charge separation. Specifically, we derived an alternative detection scheme that combines tailored lattice designs with time-of-flight probings. The latter allowed to accurately reveal the presence of each of the three SSB phases that can occur in 1D fermionic systems. It is worthwhile to underline that proposals aimed to explore the SSB, CDW, and BOW phases have been mainly based on trapping magnetic atoms into 1D optical lattices [48,49], where the subwavelength separations required to enhance the interaction strength pose a challenge for quantum gas microscopy. In this regard, our proposed scheme, combined with the recently introduced technique of the quantum gas magnifier [50], might thus represent a more feasible and flexible strategy. Other approaches to obtain extended interactions would be the use of Rydberg atoms [51,52] or dipolar molecules [53,54] trapped in optical lattices. Although these phases do not allow for a description in terms of local order parameters, they are still characterized by the phenomenon of symmetry breaking that our proposed method might detect efficiently. In conclusion, our results open up avenues in the comprehension and detection of spontaneously symmetry-broken states of matter.

Acknowledgments. We thank T. Esslinger for useful discussions. The numerical calculations were performed using the TenPy Library [55]. K.G.-L. acknowledges the Catalonia Quantum Academy (CQA). The ICFO group acknowledges support from ERC AdG NOQIA; MICIN/AEI (PGC2018-0910.13039/501100011033, CEX2019-000910-S/10.13039/501100011033, Plan National FIDEUA PID2019-106901GB-I00, FPI); MICIIN with funding from European Union NextGeneration EU (PRTR-C17.I1): QUANTERA MAQS PCI2019-111828-2;

MCIN/AEI/10.13039/501100011033 and by the European Union NextGeneration EU/PRTR QUANTERA DYNAMITE PCI2022-132919 within the QuantERA II Programme that has received funding from the European Union's Horizon 2020 research and innovation program under Grant Agreement No. 101017733 Proyectos de I+D+I Retos Colaboración QUSPIN RTC2019-007196-7; Fundació Cellex; Fundació Mir-Puig; Generalitat de Catalunya (European Social Fund FEDER and CERCA program, AGAUR Grant No. 2021 SGR 01452, QuantumCAT U16-011424, co-funded by ERDF Operational Program of Catalonia 2014-2020); Barcelona Supercomputing Center MareNostrum (FI-2023-1-0013); EU (PASQuanS2.1, 101113690); EU Horizon 2020 FET-OPEN OPTOlogic (Grant No. 899794); EU Horizon Europe Program (Grant Agreement No. 101080086–NeQST); National Science Centre, Poland (Symfonia Grant No. 2016/20/W/ST4/00314); ICFO Internal QuantumGaudi project; European Union's Horizon 2020 research and innovation program under the Marie-Skłodowska-Curie Grant Agreements No. 101029393 (STREDCH) and No. 847648 (La Caixa Junior Leaders fellowships ID100010434: LCF/BQ/PI19/11690013, LCF/BQ/PI20/11760031, LCF/BQ/PR20/11770012, LCF/BQ/PR21/11840013). C.W. acknowledges funding by the Cluster of Excellence "CUI: Advanced Imaging of Matter" of the Deutsche Forschungsgemeinschaft (DFG) - EXC 2056 - Project ID No. 390715994, by the DFG Research Unit FOR 2414, Project No. 277974659, and by the European Research Council (ERC) under the European Union's Horizon 2020 research and innovation program under Grant Agreement No. 802701. L.B. acknowledges financial support within the DiQut Grant No. 2022523NA7 funded by European Union NextGeneration EU, PRIN 2022 program (D.D. 104 - 02/02/2022 Ministero dell'Universitá e della Ricerca). J.A.-L. acknowledges support by the Spanish Ministerio de Ciencia e Innovación (MCIN/AEI/10.13039/501100011033, Grant No. PID2023-147469NB-C21), and by the Generalitat de Catalunya (Grant No. 2021 SGR 01411).

Views and opinions expressed are those of the authors only and do not necessarily reflect those of the European Union, European Commission, European Climate, Infrastructure, and Environment Executive Agency (CINEA), or any other granting authority. Neither the European Union nor any granting authority can be held responsible for them.

[1] W. Ludwig and C. Falter, *Symmetries in Physics: Group Theory Applied to Physical Problems*, 2nd ed. (Springer, Berlin, 1996).

[2] A. J. Beekman, L. Rademaker, and J. van Wezel, An introduction to spontaneous symmetry breaking, SciPost Phys. Lect. Notes **11**, (2019).

[3] J. Fröhlich, Phase transitions, spontaneous symmetry breaking, and Goldstone's theorem, in *Encyclopedia of Condensed Matter Physics*, 2nd ed., edited by T. Chakraborty (Academic Press, Oxford, 2024), pp. 158–173.

[4] P. C. Hohenberg, Existence of long-range order in one and two dimensions, Phys. Rev. **158**, 383 (1967).

[5] N. D. Mermin and H. Wagner, Absence of ferromagnetism or antiferromagnetism in one- or two-dimensional isotropic Heisenberg models, Phys. Rev. Lett. **17**, 1133 (1966).

[6] L. D. Landau, E. M. Lifshitz, and M. Pitaevskii, *Statistical Physics* (Butterworth-Heinemann, New York, 1999).

[7] M. Lewenstein, A. Sanpera, and V. Ahufinger, *Ultracold Atoms in Optical Lattices: Simulating Quantum Many-Body Systems*, 2nd ed. (Oxford University Press, Oxford, 2017).

[8] I. Bloch, J. Dalibard, and W. Zwerger, Many-body physics with ultracold gases, Rev. Mod. Phys. **80**, 885 (2008).

[9] L. Su, A. Douglas, M. Szurek, R. Groth, S. F. Ozturk, A. Krahn, A. H. Hébert, G. A. Phelps, S. Ebadi, S. Dickerson, F. Ferlaino, O. Marković, and M. Greiner, Dipolar quantum solids emerging in a Hubbard quantum simulator, Nature (London) **622**, 724 (2023).

[10] H. P. Zahn, V. P. Singh, M. N. Kosch, L. Asteria, L. Freystatzky, K. Sengstock, L. Mathey, and C. Weitenberg, Formation of spontaneous density-wave patterns in dc driven lattices, Phys. Rev. X **12**, 021014 (2022).

[11] L. Tanzi, S. M. Roccuzzo, E. Lucioni, F. Famá, A. Fioretti, C. Gabbanini, G. Modugno, A. Recati, and S. Stringari, Supersolid symmetry breaking from compressional oscillations in a dipolar quantum gas, Nature (London) **574**, 382 (2019).

[12] M. Guo, F. Böttcher, J. Hertkorn, J.-N. Schmidt, M. Wenzel, H. P. Büchler, T. Langen, and T. Pfau, The low-energy Goldstone mode in a trapped dipolar supersolid, Nature (London) **574**, 386 (2019).

[13] L. Chomaz, D. Petter, P. Ilzhöfer, G. Natale, A. Trautmann, C. Politi, G. Durastante, R. M. W. van Bijnen, A. Patscheider, M. Sohmen, M. J. Mark, and F. Ferlaino, Long-lived and transient supersolid behaviors in dipolar quantum gases, Phys. Rev. X **9**, 021012 (2019).

[14] A. Mazurenko, C. S. Chiu, G. Ji, M. F. Parsons, M. Kanász-Nagy, R. Schmidt, F. Grusdt, E. Demler, D. Greif, and M. Greiner, A cold-atom Fermi-Hubbard antiferromagnet, Nature (London) **545**, 462 (2017).

[15] P. Scholl, M. Schuler, H. J. Williams, A. A. Eberharter, D. Barredo, K.-N. Schymik, V. Lienhard, L.-P. Henry, T. C. Lang, T. Lahaye, A. M. Läuchli, and A. Browaeys, Quantum simulation of 2D antiferromagnets with hundreds of Rydberg atoms, Nature (London) **595**, 233 (2021).

[16] H.-J. Shao, Y.-X. Wang, D.-Z. Zhu, Y.-S. Zhu, H.-N. Sun, S.-Y. Chen, C. Zhang, Z.-J. Fan, Y. Deng, X.-C. Yao, Y.-A. Chen, and J.-W. Pan, Observation of the antiferromagnetic phase transition in the fermionic Hubbard model, arXiv:2402.14605.

[17] C. Gross and W. S. Bakr, Quantum gas microscopy for single atom and spin detection, Nat. Phys. **17**, 1316 (2021).

[18] W. S. Bakr, J. I. Gillen, A. Peng, S. Fölling, and M. Greiner, A quantum gas microscope for detecting single atoms in a Hubbard-regime optical lattice, Nature (London) **462**, 74 (2009).

[19] J. F. Sherson, C. Weitenberg, M. Endres, M. Cheneau, I. Bloch, and S. Kuhr, Single-atom-resolved fluorescence imaging of an atomic Mott insulator, Nature (London) **467**, 68 (2010).

[20] M. Boll, T. A. Hilker, G. Salomon, A. Omran, J. Nespolo, L. Pollet, I. Bloch, and C. Gross, Spin- and density-resolved

microscopy of antiferromagnetic correlations in Fermi-Hubbard chains, Science **353**, 1257 (2016).

[21] T. A. Hilker, G. Salomon, F. Grusdt, A. Omran, M. Boll, E. Demler, I. Bloch, and C. Gross, Revealing hidden antiferromagnetic correlations in doped Hubbard chains via string correlators, Science **357**, 484 (2017).

[22] J. Vijayan, P. Sompet, G. Salomon, J. Koepsell, S. Hirthe, A. Bohrdt, F. Grusdt, I. Bloch, and C. Gross, Time-resolved observation of spin-charge deconfinement in fermionic Hubbard chains, Science **367**, 186 (2020).

[23] S. Baier, M. J. Mark, D. Petter, K. Aikawa, L. Chomaz, Z. Cai, M. Baranov, P. Zoller, and F. Ferlaino, Extended Bose-Hubbard models with ultracold magnetic atoms, Science **352**, 201 (2016).

[24] J. Fraxanet, D. González-Cuadra, T. Pfau, M. Lewenstein, T. Langen, and L. Barbiero, Topological quantum critical points in the extended Bose-Hubbard model, Phys. Rev. Lett. **128**, 043402 (2022).

[25] M. Sohmen, M. J. Mark, M. Greiner, and F. Ferlaino, A ship-in-a-bottle quantum gas microscope setup for magnetic mixtures, SciPost Phys. **15**, 182 (2023).

[26] E. Altman, E. Demler, and M. D. Lukin, Probing many-body states of ultracold atoms via noise correlations, Phys. Rev. A **70**, 013603 (2004).

[27] S. Fölling, F. Gerbier, A. Widera, O. Mandel, T. Gericke, and I. Bloch, Spatial quantum noise interferometry in expanding ultracold atom clouds, Nature (London) **434**, 481 (2005).

[28] I. B. Spielman, W. D. Phillips, and J. V. Porto, Mott-insulator transition in a two-dimensional atomic Bose gas, Phys. Rev. Lett. **98**, 080404 (2007).

[29] C. Carcy, H. Cayla, A. Tenart, A. Aspect, M. Mancini, and D. Clément, Momentum-space atom correlations in a Mott insulator, Phys. Rev. X **9**, 041028 (2019).

[30] T. Rom, T. Best, D. van Oosten, U. Schneider, S. Fölling, B. Paredes, and I. Bloch, Free fermion antibunching in a degenerate atomic Fermi gas released from an optical lattice, Nature (London) **444**, 733 (2006).

[31] M. Messer, R. Desbuquois, T. Uehlinger, G. Jotzu, S. Huber, D. Greif, and T. Esslinger, Exploring competing density order in the ionic Hubbard model with ultracold fermions, Phys. Rev. Lett. **115**, 115303 (2015).

[32] S. Tomonaga, Remarks on Bloch's method of sound waves applied to many-Fermion problems, Prog. Theor. Phys. **5**, 544 (1950).

[33] J. Luttinger, An exactly soluble model of a many-Fermion system, J. Math. Phys. **4**, 1154 (1963).

[34] T. Giamarchi, *Quantum Physics in One Dimension* (Oxford University Press, New York, 2004).

[35] M. Nakamura, Tricritical behavior in the extended Hubbard chains, Phys. Rev. B **61**, 16377 (2000).

[36] L. Barbiero, A. Montorsi, and M. Roncaglia, How hidden orders generate gaps in one-dimensional fermionic systems, Phys. Rev. B **88**, 035109 (2013).

[37] See Supplemental Material at http://link.aps.org/supplemental/10.1103/PhysRevResearch.6.L042048 for further details on the derivations of the NCMs.

[38] A. Impertro, S. Karch, J. F. Wienand, S. Huh, C. Schweizer, I. Bloch, and M. Aidelsburger, Local readout and control of current and kinetic energy operators in optical lattices, Phys. Rev. Lett. **133**, 063401 (2024).

[39] S. Nascimbène, Y.-A. Chen, M. Atala, M. Aidelsburger, S. Trotzky, B. Paredes, and I. Bloch, Experimental realization of plaquette resonating valence-bond states with ultracold atoms in optical superlattices, Phys. Rev. Lett. **108**, 205301 (2012).

[40] V. Guarrera, N. Fabbri, L. Fallani, C. Fort, K. M. R. van der Stam, and M. Inguscio, Noise correlation spectroscopy of the broken order of a Mott insulating phase, Phys. Rev. Lett. **100**, 250403 (2008).

[41] R. Bach and K. Rzążewski, Correlations in atomic systems: Diagnosing coherent superpositions, Phys. Rev. Lett. **92**, 200401 (2004).

[42] M. Fabrizio, A. O. Gogolin, and A. A. Nersesyan, From band insulator to Mott insulator in one dimension, Phys. Rev. Lett. **83**, 2014 (1999).

[43] A. A. Aligia, A. Anfossi, L. Arrachea, C. Degli Esposti Boschi, A. O. Dobry, C. Gazza, A. Montorsi, F. Ortolani, and M. E. Torio, Incommmensurability and unconventional superconductor to insulator transition in the Hubbard model with bond-charge interaction, Phys. Rev. Lett. **99**, 206401 (2007).

[44] N. Baldelli, A. Montorsi, S. Julià-Farré, M. Lewenstein, M. Rizzi, and L. Barbiero, Deconfined quantum critical points in fermionic systems with spin-charge separation, arXiv:2407.04073.

[45] G. I. Japaridze and E. Müller-Hartmann, Triplet superconductivity in a one-dimensional ferromagnetic *t-J* model, Phys. Rev. B **61**, 9019 (2000).

[46] A. W. Sandvik, L. Balents, and D. K. Campbell, Ground state phases of the half-filled one-dimensional extended Hubbard model, Phys. Rev. Lett. **92**, 236401 (2004).

[47] For each of those phases, both symmetry sectors are degenerate in the thermodynamic limit. However, in a real experiment one of the symmetry sectors will be preferred by imperfections, the state preparation, and/or finite-size effects. To account for this, the degeneracy breaks in our tensor networks calculation with the choice of the initial state to be optimized (see Ref. [37]).

[48] M. Di Dio, L. Barbiero, A. Recati, and M. Dalmonte, Spontaneous Peierls dimerization and emergent bond order in one-dimensional dipolar gases, Phys. Rev. A **90**, 063608 (2014).

[49] S. Julià-Farré, D. González-Cuadra, A. Patscheider, M. J. Mark, F. Ferlaino, M. Lewenstein, L. Barbiero, and A. Dauphin, Revealing the topological nature of the bond order wave in a strongly correlated quantum system, Phys. Rev. Res. **4**, L032005 (2022).

[50] L. Asteria, H. P. Zahn, M. N. Kosch, K. Sengstock, and C. Weitenberg, Quantum gas magnifier for sub-lattice-resolved imaging of 3D quantum systems, Nature (London) **599**, 571 (2021).

[51] E. Guardado-Sanchez, B. M. Spar, P. Schauss, R. Belyansky, J. T. Young, P. Bienias, A. V. Gorshkov, T. Iadecola, and W. S. Bakr, Quench dynamics of a Fermi gas with strong nonlocal interactions, Phys. Rev. X **11**, 021036 (2021).

[52] P. Weckesser, K. Srakaew, T. Blatz, D. Wei, D. Adler, S. Agrawal, A. Bohrdt, I. Bloch, and J. Zeiher, Realization

of a Rydberg-dressed extended Bose Hubbard model, arXiv:2405.20128.

[53] N. Bigagli, W. Yuan, S. Zhang, B. Bulatovic, T. Karman, I. Stevenson, and S. Will, Observation of Bose-Einstein condensation of dipolar molecules, Nature (London) **631**, 289 (2024).

[54] J. S. Rosenberg, L. Christakis, E. Guardado-Sanchez, Z. Z. Yan, and W. S. Bakr, Observation of the Hanbury Brown–Twiss effect with ultracold molecules, Nat. Phys. **18**, 1062 (2022).

[55] J. Hauschild and F. Pollmann, Efficient numerical simulations with tensor networks: Tensor Network Python (TeNPy), SciPost Phys. Lect. Notes **5** (2018).